

Tracking propagation of ultrashort intense laser pulses in gases via probing of ionization

L. A. Gizzi,^{1,2,*} S. Betti,^{1,2} M. Galimberti,^{1,†} A. Giulietti,^{1,2,‡} D. Giulietti,^{1,2} L. Labate,^{1,2} T. Levato,^{1,2} P. Tomassini,^{1,2,§} P. Monot,³ T. Ceccotti,³ P. De Oliveira,³ and Ph. Martin³¹*Intense Laser Irradiation Laboratory, IPCF-Area della Ricerca CNR, Via Moruzzi, 1 56124 Pisa, Italy*²*Istituto Nazionale di Fisica Nucleare-INFN, Pisa, Italy*³*Physique à Haute Intensité, CEA-DSM/DRECAM/SPAM, Bât. 522 p. 148, 91191 Gif sur Yvette Cedex, France*

(Received 7 October 2008; revised manuscript received 1 February 2009; published 26 May 2009)

We use optical interferometry to study the propagation of femtosecond laser pulses in gases. We show the measurements of propagation in a nitrogen gas jet and we compare the results with propagation in He under the same irradiation conditions. We find that in the case of nitrogen, the detailed temporal structure of the laser pulse can be tracked and visualized by measuring the phase and the resulting electron-density map. A dramatically different behavior occurs in He gas jets, where no details of the temporal structure of the laser pulse are visible. These observations are explained in terms of the ionization dynamics of nitrogen compared to helium. These circumstances make N₂ gas sensitive to variations in the electric field and, therefore, allow the laser-pulse temporal and spatial structures to be visualized in detail.

DOI: [10.1103/PhysRevE.79.056405](https://doi.org/10.1103/PhysRevE.79.056405)

PACS number(s): 52.50.Jm, 52.25.Jm, 52.70.Kz

I. INTRODUCTION

The interaction of short and ultrashort laser pulses in gas jets is under continuing extensive investigation for its potential for a wide range of studies and applications. Well-established optical interferometry techniques can, by measuring the phase shift induced on a probe pulse, provide space-resolved information at the submicrometer scale on a variety of physical systems. Laser-induced plasmas are among the most common systems investigated with the help of this technique [1]. Provided a sufficiently short probe pulse is used, the evolution of the plasma electron density can be followed on an ultrafast time scale using a pump-and-probe-like approach. Similar techniques have already been successfully applied to time-resolved analysis of several phenomena including, for example, channel formation in gas jets [2], radiative blast waves [3], and characterization of plasma precursor effects in the interaction of chirped pulse amplification (CPA) [4] laser pulses with solids [5]. These systems are extensively exploited for the investigation of a wide range of phenomena in both fundamental and applied sciences including the generation of ultrashort pulses of radiation from the UV [6] to the x-ray range [7], laser-driven acceleration of charged particles [8], and benchmarking of high-field-ionization [9] models. In this class of experiments a variety of additional optical techniques including blueshift analysis [10,11] and frequency resolved optical gating [12] is also used to acquire information on the dynamics of ionization.

In this work we use probing measurements under well-known interaction conditions to extract information on the laser pulse propagating in the gas jet. In particular, we compare ionization in nitrogen and helium under similar irradiation

conditions, showing how the different He and N atomic structure can play a role in interferometric measurements and how they can allow the spatial-temporal structure of the laser pulse to be reconstructed. This, in turn, effectively illustrates the potential of this measurement to perform a semiquantitative single-shot monitoring of CPA femtosecond laser pulses. Our measurements reveal unexpected features of the ionization map that appear to be sensitive to the detailed structure of the laser pulse in the interaction region. Occurrence of these features in similar experimental configurations may partially account for the poor control and reproducibility of a variety of applications, including, for example, laser-plasma acceleration and high-order harmonic generation.

The paper is organized as follows. In Sec. II we describe the experimental setup and discuss the main limitations, also in view of previous modeling work [13] and precursor experiments [14]. Section III is dedicated to the presentation of the experimental observations and, in particular, to the comparison of the electron-density maps in N₂ and in He, which have been extracted from plasma interferograms using well-established analysis techniques [15]. Then, in Sec. IV, we describe the model of ionization used to analyze our experimental density maps and the numerical simulations performed, providing a basic characterization of ionization in He and N₂ gases. Finally, in Sec. V we present our conclusions.

II. EXPERIMENTAL SETUP AND FRINGE PATTERNS

The experiment was performed at the SLIC laser facility at the Saclay Centre of CEA (France) with the 10 TW UHI10 laser system. The Ti:Sa laser system operates in the CPA mode and delivers up to 0.6 J in 60-fs laser pulses at 800 nm. The nanosecond contrast, due to the amplified spontaneous emission (ASE), was found to be $\approx 10^6$, while the picosecond pedestal of the femtosecond pulse had a level of $\approx 10^{-4}$ for a duration of about 1 ps before the main pulse. The main pulse was focused in the gas jet using a 200 mm focal length, silver coated off-axis parabolic mirror. The numerical aper-

*Corresponding author.

†Present address: Central Laser Facility, Rutherford Appleton Laboratory, Didcot, Oxon, UK.

‡Also at: Physics Department “E. Fermi”, Pisa University, Italy.

§Present address: INFN, Sez. Milano, Italy.

ture of the focusing optics was $f/2.5$, and the maximum focused nominal intensity was 10^{19} W cm $^{-2}$ in a slightly elliptical focal spot whose horizontal and vertical diameters were 8 μm and 10 μm full width at half maximum (FWHM), respectively. The corresponding maximum normalized field parameter in the focal spot was $a_0=2.6$. The gas jet was delivered by a 1 mm diameter cylindrical nozzle with the laser pulse propagating at a distance of 200 μm from the tip and along a diameter of the nozzle. The gas pressure in the valve was 8 bar, resulting in a maximum neutral density around 10^{20} atoms/cm 3 . A detailed study of ionization in He is described elsewhere [14]. Here we present results obtained in nitrogen and we discuss the main differences with respect to those obtained in He. The waist of the laser pulse was set to be at the boundary of the jet, where the gas density is sufficiently low to prevent plasma formation by the precursor ASE radiation. These circumstances were systematically verified as described elsewhere [16].

A fraction of the main femtosecond pulse was frequency-doubled by a 2 mm thick type I KDP crystal and used as an optical probe propagating perpendicular to the main pulse, in a Mach-Zehnder interferometer configuration. The probe pulse duration was estimated to be 130 fs FWHM, with a pulse shape close to a second-order super-Gaussian profile. A test of the performance of the interferograms was carried out, measuring the refractive index of neutral He gas, showing that phase shift up to one tenth of a wavelength could be detected [17] from Fourier analysis [18,9] of the measured fringe pattern.

The propagation of the laser pulse in the gas was measured in a ‘‘pump-and-probe’’-like approach, i.e., by taking a series of interferograms varying shot by shot the probe pulse-to-main-pulse delay, with a time step as short as 60 fs. The images of Fig. 1 show a sequence of three interferograms of propagation in N $_2$, taken at probe times starting at 1.00 ps, where probe time zero is conventionally defined as the time at which the CPA pulse is at the position of the waist.

At these times the pulse has just passed the waist position and the fringe pattern show perturbation in a conelike shaped area, with an aperture of roughly 25 $^\circ$, corresponding to the full aperture of the focusing optics as indicated by the dashed line that marks the $1/e^2$ profile of the beam, assuming Gaussian propagation with an $M^2=2.3$. The longitudinal extent of the perturbed region in the fringe pattern of frame (c) is roughly 700 μm , measured from the waist position. This value is in a good agreement with the value expected for propagation at the speed of light starting from the position of the waist at probe time zero. In fact, the whole sequence of interferometric maps (not shown here) shows a fringe perturbation front proceeding at the speed of light up to a probe delay time of 3 ps.

III. PHASE EXTRACTION AND DENSITY MAPS

A quantitative evaluation of the electron density requires a phase map extraction from the fringe patterns of Fig. 1. Fourier transform analysis was applied as discussed in [9], where the intensity of the fringe pattern on the detector plane (x,y) is written as

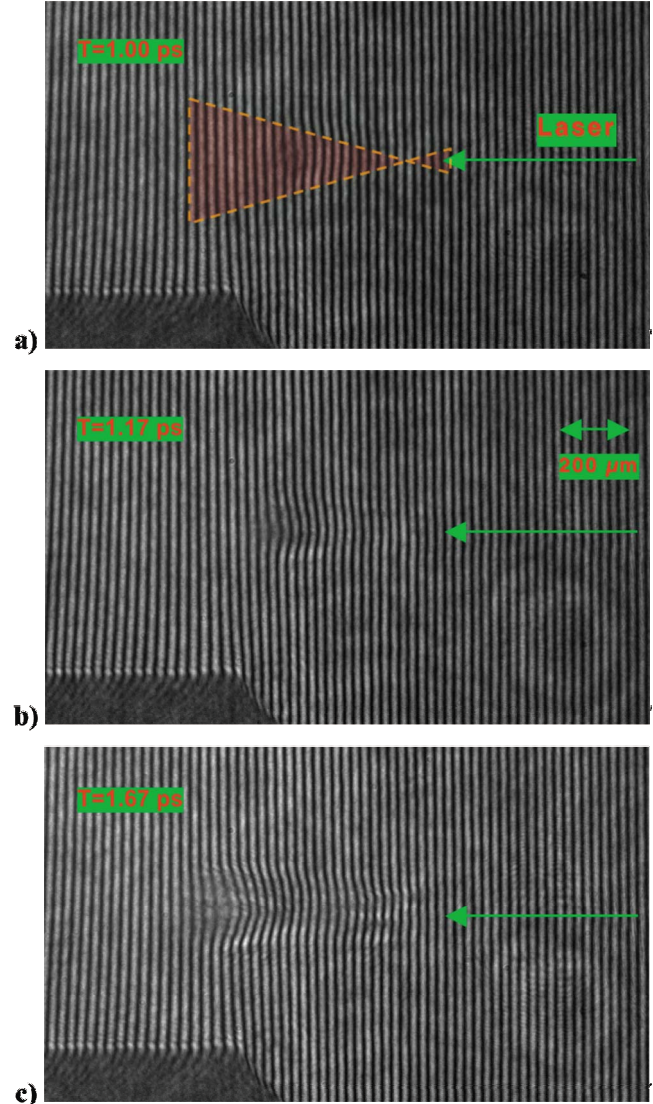


FIG. 1. (Color online) Interferogram of laser propagation in N $_2$ (eight bars) taken at three different probing times as indicated in the figure. The laser pulse propagates from right to left and the dashed line in the frame (a) shows the $1/e^2$ profile assuming Gaussian propagation and $M^2=2.3$. The dark trapezoid-shaped region visible in the lower-left corner is the tip of the conical gas-jet nozzle. Fringe shift (to the right) visible in the center of the image frames correspond to phase shift induced by the plasma produced by the laser pulse. Fringe shift in the opposite direction (to the left) just visible above the nozzle are due to phase shift induced by the neutral nitrogen atoms.

$$I(x,y) = a(x,y) + [c(x,y)\exp(2\pi if_u x) + \text{c.c.}],$$

where

$$c(x,y) = 1/2b(x,y)\exp[i\Delta\varphi(x,y)]$$

and its complex conjugate carry the information on phase shift $\Delta\varphi(x,y)$, background intensity $a(x,y)$, and fringe visibility $b(x,y)$. This intensity pattern can be processed using Fourier transform analysis to obtain a complex array whose

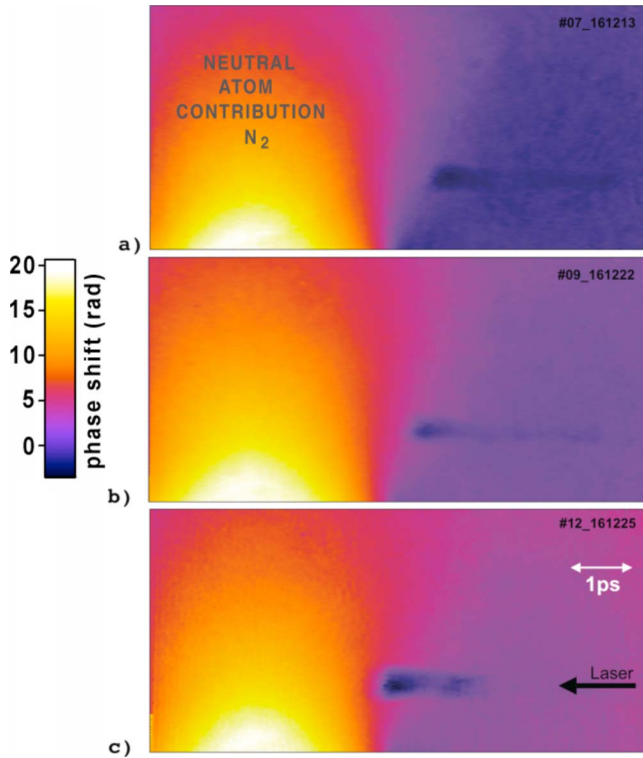


FIG. 2. (Color online) Phase maps of the interferograms of Fig. 1 showing propagation in nitrogen gas jet taken (from top to bottom) at probe time +1 ps, +1.17 ps, and +1.67 ps. The CPA beam propagates from the right to the left. The neutral atom (positive) contribution to the phase shift is clearly visible on the left (lighter colors), while the free-electron contribution due to laser-pulse propagation is visible as darker colors.

imaginary part is the phase map $\Delta\varphi(x, y)$ and the visibility of the fringes, $b(x, y)$.

The image of Fig. 2 shows three successive phase maps taken from the interferogram images of Fig. 1, at +1 ps, +1.17 ps, and +1.67 ps. Visible in the left-hand side of each of the three frames is the phase shift due to the neutral nitrogen atoms of the gas jet. According to these images, as the pulse propagates (from right to left), the ionization front moves ahead with the speed of light. As the gas density

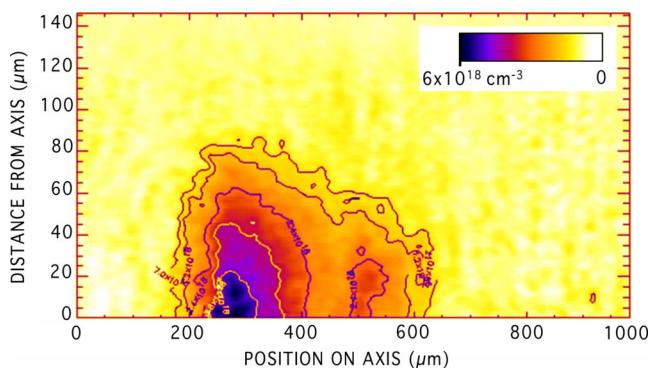


FIG. 3. (Color online) Electron-density map obtained from Abel inversion of the phase map of Fig. 2 taken at +1.67 ps. The absolute value of the electron density is indicated in the color bar.

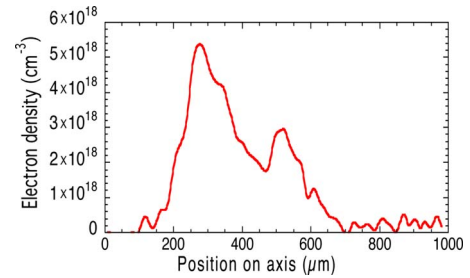


FIG. 4. (Color online) Lineout of the electron density taken on the axis of the density map of Fig. 3 showing the two peaks of electron density separated by 250 μm .

increases along the laser-pulse propagation path, the phase shift due to the leading edge of the pulse increases and the trailing part of the pulse becomes visible. A second localized peak of ionization, separated from the front by approximately 1 ps, appears in the frame (c). This feature can be more accurately observed in the electron-density map obtained by Abel inversion of the 1.67 ps phase map and shown in Fig. 3. A lineout of such electron-density map taken on the pulse symmetry axis, shown in Fig. 4, clearly shows the presence of the two localized density peaks.

In contrast, a significantly different result is found in the case of propagation in a Helium gas jet under the same laser configuration. Figure 5 shows the interferogram obtained in helium case at the same probing time as frame (c) of Fig. 2, showing a regular conelike structure that reproduces the expanding laser beam path, as shown by the dashed line, with no evidence of secondary ionization peaks.

The behavior of ionization in helium which is observed in our experiment, including the occurrence of a significant loss of fringe visibility due to transient ultrafast ionization, has been extensively described elsewhere [14,16]. Here we will be only concerned with the difference in the ionization dynamics of N_2 with respect to that of He as originating from the different atomic structure of the two species. The following section is dedicated to a description of ionization properties of these two elements and to a modeling of the observed experimental results.

IV. IONIZATION IN VERY INTENSE FIELDS: HELIUM VS. NITROGEN

We now consider the properties of ionization of He and N atoms starting from their basic atomic properties. In particular, we will essentially be concerned with the atomic structure of the two species and the associated ionization potentials, which, for both elements, are summarized in Table I.

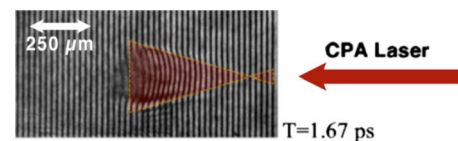


FIG. 5. (Color online) Interferogram of the plasma generated by CPA in a Helium gas jet. The interferogram was taken at the same time of 1.67 ps as the interferogram (c) of Fig. 1.

TABLE I. Ionization potentials of He and N. The second row gives the ionization energy of nitrogen from neutral to hydrogenlike N. The third row reports the corresponding ionization energies for neutral He and hydrogenlike He.

Atom	Neutral (eV)	+1 (eV)	+2 (eV)	+3 (eV)	+4 (eV)	+5 (eV)	+6 (eV)
N	14.53	29.60	47.45	77.48	97.89	552.1	667.1
He	24.59	54.42					

According to Table I, the first ionization energy of nitrogen atoms is significantly smaller than the corresponding energy of He. Also, in the case of N, there are five successive ionization stages with a gradually increasing energy up to about 40 times the first ionization threshold. This is markedly different from the behavior of He, whose two ionization energies only differ by a factor of roughly two. Therefore, we expect that, compared with He, ionization in N_2 will occur at a much lower laser intensity. Furthermore, due to the higher number of electrons per atom, higher field values are needed to reach full ionization in N_2 compared to He.

This behavior will provide an effective greater dynamic range in the response of ionization to the laser field strength. A quantitative evaluation of this effect in our experimental conditions has been carried out using a numerical simulation code based upon a tunnel ionization model [19]. In the numerical code, the pulse propagates into a gas of uniform density according to the simple Gaussian optics propagation and no account is taken of nonlinear propagation effects. As for the self-focusing, we can reasonably rule this out as the maximum laser power is below the critical power for relativistic self-focusing. In fact, according to Fig. 4, the maximum electron density at the position of the laser beam waist, located approximately at $600 \mu\text{m}$, is of the order of 10^{18} cm^{-3} . According to the well-known relationship [20,21] for critical power for relativistic self-focusing $P_{cr} \cong 17(\omega/\omega_p)^2 \text{GW}$, the critical power is above 30 TW, which is well above the maximum available laser power. At

the peak available density of $5 \times 10^{18} \text{ cm}^{-3}$, corresponding to a critical power of 6 TW, the laser pulse is expanding well beyond the beam waist and has already undergone significant depletion due to absorption due to ionization and diffusion. Under these circumstances we can, therefore, rule out possible contributions of relativistic self-focusing effects in our experiment and we can focus our investigation on pure ionization effects.

The ionization maps of Fig. 6 show the results obtained in He (left) and N_2 (right), at peak laser intensities of $3 \times 10^{18} \text{ W/cm}^2$ and $3 \times 10^{15} \text{ W/cm}^2$, respectively. According to these results, the ionization profile obtained for propagation in nitrogen is almost the same as that obtained in helium with a laser-pulse intensity 10^3 times higher. In fact, according to the color tables of the two frames, the maximum ionization degree in nitrogen is 1.2, compared with the maximum ionization degree of 1 obtained in helium. In other words, in this laser intensity regime, nitrogen is capable of showing the same ionization effects of helium at a laser field intensity three orders of magnitude lower. In addition, the larger number of electrons of nitrogen compared to helium makes it possible to explore higher laser fields.

We hereby show how these features can be exploited to recover the temporal and spatial structure of the laser pulse from ionization maps like the one of Fig. 3. In particular, we could explain the secondary ionization peak of Fig. 3, spatially separated from the main one of roughly $300 \mu\text{m}$, as due to the presence of a post pulse in the laser temporal profile. In fact, according to the detailed temporal structure of the pulse as obtained from the third-order autocorrelation measurement shown in Fig. 7, a post pulse is visible one picosecond after the main pulse, whose intensity relative to the main pulse is of the order of roughly $1/5$, whose duration is of the order of half of that of the main pulse.

Nevertheless, the assumption of a low-intensity post pulse cannot, by itself, explain the observed longitudinal double-peak structure in the electron density of Fig. 3. In fact, in a double-pulse configuration, as the first pulse propagates in the laser Rayleigh length, a semicolumn of plasma like the one displayed in Fig. 6 is formed at a given time. A post

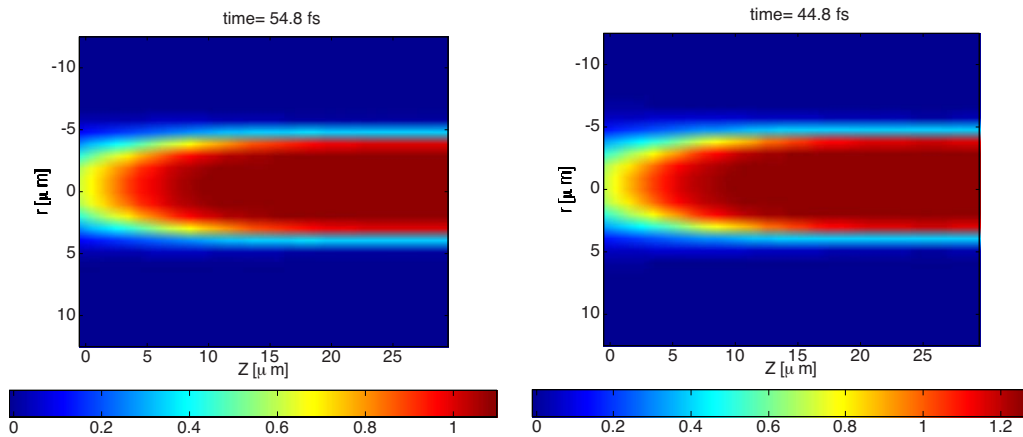


FIG. 6. (Color online) Calculated ionization produced by a 70 fs laser pulse propagating (to the left) in a uniform gas density of $1.5 \times 10^{18} \text{ atoms/cm}^3$. The map on the left was obtained considering a pulse energy of 100 mJ laser pulse propagating in a helium gas. The map on the right was obtained considering a pulse energy of 0.1 mJ propagating in a nitrogen gas. The calibration bar of the nitrogen map (rhs) was adjusted to make both color maps identical.

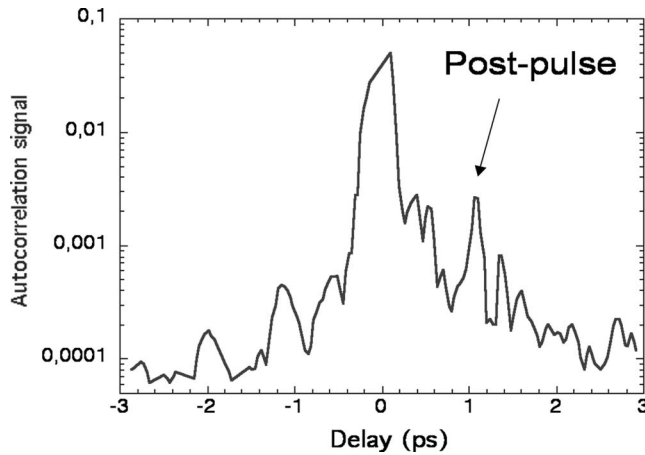


FIG. 7. Third-order autocorrelation trace of the CPA pulse showing the main pulse and the detailed structure of the pulse on the picosecond time scale.

pulse, separated by a given delay, say 1 ps, would only generate a similar column, superimposed to the first one, with the ionization fronts separated by 300 ps (assuming propagation at the speed of light). In our case, therefore, the post pulse would only lead to a small step-wise increase in the ionization profile generated by the preceding main pulse.

A possible explanation of the result displayed in Fig. 3 is that along with the double-pulse structure of Fig. 7, we also assume that the post pulse is focusing at a different position (i.e., has a slightly different beam divergence) than the main pulse, reaching there an intensity exceeding that of the main pulse at the same position. A detailed discussion of the origin of such a double-pulse structure is beyond the scope of the present work. Here we only point out that, in general, post pulses may arise, from spurious reflections of the main pulse in the laser chain. A 1 ps delay between pulses corresponds to an optical path of 300 μm that may arise, for example, from a secondary reflection by a 100 μm glass plate. A post pulse may also arise from birefringence of a Ti:Sa crystal in the main amplifier due to the amplification of a small fraction of the main pulse along the slow axis of the crystal. In this case, difference in the thermal lensing or collimation of the beam in the crystal may explain a difference in the divergence of the post pulse. We point out here that such an effect is by no means easy to characterize using conventional laser measurements and the technique proposed in our manuscript could indeed be used to perform dedicated measurements on the focusing properties of temporally structured laser pulses.

This specific scenario was modeled using the ionization code presented above. We carried out a set of numerical simulations in which a 100 mJ, 60 fs main pulse followed by a 10 mJ 30 fs post pulse were delivered onto an initially neutral N_2 gas in order to investigate the resulting ionization profile. In the simulation, the pulses had Gaussian profiles both in space and time, and the distance between the focal points of the two pulses was 450 μm . An $M^2=2.3$ was included in the calculations to account for real-beam propagation. With these parameters, at the post-pulse focal point the intensity of the post pulse is higher than that of the main

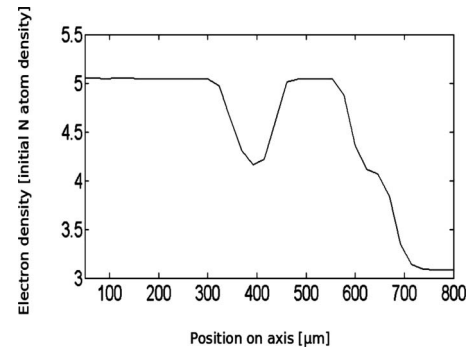


FIG. 8. Normalized electron-density profile on axis for nitrogen as a function of the position obtained in a numerical simulation in which a 100 mJ 60 fs main pulse was followed by a 10 mJ 30 fs post-pulse. The main and the post-pulse focal points are placed at $x=50 \mu\text{m}$ and $x=500 \mu\text{m}$, respectively.

pulse by approximately a factor of 4. The calculated electron-density profile obtained from the simulations is plotted in Fig. 8, in units of the initial density of the neutral nitrogen atoms. The electron-density pattern obtained from the simulation shows the presence of two spatially separated regions of ionization consistent with the assumed separate focal regions of the main pulse and the post pulse. Note that, in the case discussed, the presence of a post-pulse allows, at the post-pulse focal point, an increase in the local ionization degree of nitrogen from 4 to 5. As pointed out above, the high-ionization dynamics of nitrogen (with respect to helium) allows the post pulse to further ionize the medium, producing a secondary ionization peak. This behavior is qualitatively consistent with the experimental electron-density profile of Fig. 4, while the amplitudes of the two peaks of electron density obtained experimentally are quantitatively different, as the simulation tends to overestimate the ionization.

Additional explanation of the discrepancy between the numerical and the experimental results is to be attributed to the fact that in our numerical code the pulses propagate in a uniform density gas density, compared to the experiment in which the gas density is maximum on the axis of the nozzle and decreases monotonically toward the edge. Therefore, the main pulse focuses in a region in which the gas density is higher than that in the focal point of the post pulse, thus, producing a higher electron density. Clearly, a quantitative comparison between modeling results and the experiment is a complex task that requires a self-consistent calculation of ionization that is beyond the aim of the present work. At this stage we can however already confirm that our assumption of the effect of a post pulse, with separate location of the focal region is consistent with the experimental measurements. This result can also be regarded as an advanced laser-pulse diagnostics that provides simultaneously detailed information on the temporal and angular properties of the laser pulse that can be exploited in different configurations to provide additional information on the laser system using a technique complementary to standard laser diagnostic techniques.

V. CONCLUSIONS

We have carried out comparative interferometric measurements of an ultrashort (60 fs) 600-mJ laser pulse propagating

into either a helium or a nitrogen gas jet. The interferometric patterns obtained in the two gases show a significantly different behavior. In particular, in case of He the main pulse is found to generate a clean ionization pattern in the gas, while in case of N₂ a richer and spatially structured ionization pattern has been observed. The nitrogen electron-density map extracted from the interferograms revealed the presence of two spatially separated ionization peaks of different amplitude. With the help of a numerical code capable of taking into account field ionization in nitrogen, we were able to show that the lower density region can be explained as originating from the presence of a low-energy post pulse, which focuses in a spatial region different from the main-pulse focal point. In this position, initially during the interaction, the intensity of the post pulse exceeds that of the main pulse and gives rise to a measurable ionization region.

These features of the laser pulse were enhanced by the response of the ionization of nitrogen to the laser field amplitude. Although the results obtained in our experiment are dependent upon the specific laser configuration used here,

comparable effects are most likely to take place in similar experimental configurations and laser systems. Our measurements show that high-quality ultrashort pulse interferometry can be profitably used to investigate such features, thus, increasing the knowledge on the temporal and spatial structure of laser pulses used in a wide range of applications to improve control and reproducibility of experiments.

ACKNOWLEDGMENTS

We would like to thank the staff of the SLIC laser facility for their invaluable and friendly support. We also thank Luc Vigroux of Amplitude Technologies for enlightening discussion concerning femtosecond laser technology. We acknowledge support from the LASERLAB EUROPE Trans-national Access Programme. We thank A. Barbini, W. Baldeschi, A. Rossi, and M. Voliani of the IPCF staff for their technical assistance. This work was partially supported by the joint INFN-CNR Project “Plasmon-X” and by the MIUR funded FIRB-SPARX project.

-
- [1] O. Willi, in *Laser-Plasma Interactions 4*, Proceedings of the XXXV SUSSP, St. Andrews, 1988, edited by M. B. Hooper (SUSSP, Edinburgh, 1989).
- [2] M. Dunne, T. Afshar-Rad, J. Edwards, A. J. MacKinnon, S. M. Viana, O. Willi, and G. Pert, *Phys. Rev. Lett.* **72**, 1024 (1994); V. Malka *et al.*, *ibid.* **79**, 2979 (1997).
- [3] M. J. Edwards, A. J. MacKinnon, J. Zweiback, K. Shigemori, D. Ryutov, A. M. Rubenchik, K. A. Keilty, E. Liang, B. A. Remington, and T. Ditmire, *Phys. Rev. Lett.* **87**, 085004 (2001).
- [4] D. Strickland and G. Mourou, *Opt. Commun.* **56**, 219 (1985).
- [5] D. Giulietti *et al.*, *Phys. Plasmas* **9**, 3655 (2002).
- [6] Y. Mairesse *et al.*, *Phys. Rev. Lett.* **93**, 163901 (2004).
- [7] A. Rousse *et al.*, *Phys. Rev. Lett.* **93**, 135005 (2004); A. Ya. Faenov *et al.*, *Laser Part. Beams* **26**, 69 (2008).
- [8] S. P. D. Mangles *et al.*, *Nature (London)* **431**, 535 (2004); C. G. R. Geddes *et al.*, *ibid.* **431**, 538 (2004); J. Faure *et al.*, *ibid.* **431**, 541 (2004); S. Betti *et al.*, *Plasma Phys. Controlled Fusion* **47**, 521 (2005); T. Ceccotti, A. Levy, H. Popescu, F. Reau, P. D’Oliveira, P. Monot, J. P. Geindre, E. Lefebvre, and P. Martin, *Phys. Rev. Lett.* **99**, 185002 (2007); F. Ceccherini *et al.*, *Laser Phys.* **16**, 594 (2006); F. Cornolti, F. Ceccherini, S. Betti, and F. Pegoraro, *Phys. Rev. E* **71**, 056407 (2005).
- [9] B. Walker, B. Sheehy, L. F. DiMauro, P. Agostini, K. J. Schafer, and K. C. Kulander, *Phys. Rev. Lett.* **73**, 1227 (1994).
- [10] D. Giulietti, L. A. Gizzi, A. Giulietti, A. Macchi, D. Teychenne, P. Chessa, A. Rousse, G. Cheriaux, J. P. Chambaret, and G. Darpentigny, *Phys. Rev. Lett.* **79**, 3194 (1997).
- [11] C. W. Siders *et al.*, *J. Opt. Soc. Am. B* **13**, 330 (1996).
- [12] C. W. Siders, G. Rodriguez, J. L. W. Siders, F. G. Omenetto, and A. J. Taylor, *Phys. Rev. Lett.* **87**, 263002 (2001).
- [13] M. Galimberti, *J. Opt. Soc. Am. A Opt. Image Sci. Vis.* **24**, 304 (2007).
- [14] L. A. Gizzi *et al.*, *Phys. Rev. E* **74**, 036403 (2006).
- [15] L. A. Gizzi, D. Giulietti, A. Giulietti, T. Afshar-Rad, V. Biancalana, P. Chessa, C. Danson, E. Schifano, S. M. Viana, and O. Willi, *Phys. Rev. E* **49**, 5628 (1994); M. Borghesi, A. Giulietti, D. Giulietti, L. A. Gizzi, A. Macchi, and O. Willi, *ibid.* **54**, 6769 (1996).
- [16] A. Giulietti, P. Tomassini, M. Galimberti, D. Giulietti, L. A. Gizzi, P. Köster, L. Labate, T. Ceccotti, P. D’Oliveira, T. Auguste, P. Monot, and Ph. Martin, *Phys. Plasmas* **13**, 093103 (2006).
- [17] L. A. Gizzi *et al.*, Proceedings of the Third international Conference on Superstrong Fields in Plasmas, AIP Conf. Proc., edited by M. Lontano *et al.* (Melville, New York, 2006), Vol. 827, p. 3.
- [18] M. Takeda, H. Ia, and S. Kobayashi, *J. Opt. Soc. Am.* **72**, 156 (1982).
- [19] G. L. Yudin and M. Y. Ivanov, *Phys. Rev. A* **64**, 013409 (2001).
- [20] G. M. Mourou *et al.*, *Rev. Mod. Phys.* **78**, 309 (2006).
- [21] M. V. Asthana *et al.*, *Phys. Scr.* **T84**, 191 (2000).